Xuemei Yang*, Hongzhen Guo, Zekun Yao and Shichong Yuan

Flow Behavior and Dynamic Recrystallization of BT25y Titanium Alloy During Hot Deformation

DOI 10.1515/htmp-2016-0100
Received January 21, 2017; accepted January 26, 2017

Abstract: The high-temperature plastic deformation and dynamic recrystallization behavior of BT25y alloy were investigated within the deformation temperatures of 1,213–1,293 K and strain rates of 0.001–1.0 s^{-1} on a Gleeble-1500 thermo-mechanical simulator. Results showed that the dynamic recrystallization (DRX) mechanism played an important role in the hot deformation of BT25y alloy. Based on the regression analysis of the true stress–strain data, the stress exponent and deformation activation energy of BT25y alloy were calculated to be 3.4912 and 288.0435 kJ/mol, respectively. The θ-σ and $d\theta/d\sigma$–σ curves were plotted to further obtain the critical stress and critical strain for the occurrence of DRX. Based on the analysis results, the DRX kinetic model was established. The model was validated by the comparison between predicted and experimental volume fraction of DRX. As the DRX evolution was sensitive to deformation temperature and strain rate, quantities of dynamically recrystallized grains appeared at higher temperatures and lower strain rates.

Keywords: BT25y alloy, hot deformation, strain hardening rate, critical strain, dynamic recrystallization

Introduction

The high-temperature BT25y titanium alloy was improved on the basis of BT25 alloy, which was developed by ВИАМ in the former Soviet Union in 1971. Its nominal composition is Ti-6.5Al-2Sn-4Zr-4Mo-1W-0.2Si. Due to the addition of β eutectoid element tungsten and neutral element stannum, the alloy possesses excellent mechanical performance combining strength, persistence and stability at the service temperature of 723–823 K. However, the Russian alloy BT25y is seldom known in the west countries, public information concerning its high-temperature deformation behavior can almost not be found. The BT25y alloy is a kind of martensitic α + β titanium alloy, which can be adopted to produce compressor disks with outstanding tensile strength and creep resistance at high temperature [1]. In recent years, increasing attentions have been paid to BT25y in China due to its potential for manufacturing dual-property blisk [2]. It is of crucial importance to study the high-temperature deformation behavior and microstructural evolution to better control the microstructures and corresponding mechanical properties during hot deformation. However, investigations on the flow behavior and deformation mechanism of BT25y alloy under elevated temperature have not been conducted yet.

The high-temperature flow behavior during hot deformation is a complex process. The work hardening (WH), dynamic recovery (DRV) and dynamic recrystallization (DRX) can occur at different deformation stages [3]. Especially, the effect of DRX mechanism on the flow behavior and microstructural evolution is significant. Therefore, understanding the relationships between DRX behavior and hot processing parameters is very necessary for the processing optimization and mechanism exploration. Thus, dynamic recrystallization has been investigated by many researchers in the last two decades. A set of mathematical models with good precision have been proposed to describe the DRX kinetics and analyze the microstructural evolution of different steels [4–8]. Recently, with the wide application of titanium alloys in aerospace industry, more and more attentions have been paid to research the deformation behavior and DRX kinetics of titanium alloys. Momeni [9] and Li [10] studied the deformed microstructures of Ti-6Al-4V and Ti-3Al-5V-5Mo alloys with different β-forging processes and found the occurrence of DRX in forged microstructures. Nan [11] obtained the critical strain for the DRX initiation of Ti-5Al-5Mo-5V-1Cr-1Fe alloy under different deformation conditions by identifying the curve inflection of work hardening rate with respect to the stress. Quan [12] established the DRX kinetic model for Ti-6Al-4V alloy based on the Johnson-Mehl-Avrami-Kolmogorov (JMAK) equation to characterize the evolution of DRX volume fraction.

***Corresponding author: Xuemei Yang,** School of Materials Science and Engineering, Northwestern Polytechnical University, Xi'an 710072, PR China, E-mail: yangxuemei@mail.nwpu.edu.cn
Hongzhen Guo, Zekun Yao, School of Materials Science and Engineering, Northwestern Polytechnical University, Xi'an 710072, PR China
Shichong Yuan, China National Erzhong Group Co., Deyang 618013, China

Tan [13] proposed an internal-variable identification approach to investigate the DRX behavior of Ti55511 alloy and found that the DRX process of Ti55511 alloy tended to occur under moderate temperatures and low strain rates. Liang [14] studied the correlation between grain size and flow stress of TC18 alloy during the steady-state DRX stage, and generalized a dynamic model of DRX evolution by proposing an identification criterion on DRX continuity or periodicity. Wu [15] simulated the discontinuous dynamic recrystallization (DDRX) of Ti-6Al-2Zr-1Mo-1V in β phase field with CA model, and the simulated results showed that DRX volume fraction decreased with increasing strain rate or decreasing temperature. Fan [16] has investigated the role of dynamic and post dynamic recrystallization on microstructure refinement in the primary working of a coarse grained two-phase titanium alloy, and found that the DRX could be triggered at a low strain in β deformation. However, descriptions for the DRX kinetics and microstructural evolution of BT25y alloy have not been performed in published literatures.

The objective of this study is to investigate the high-temperature deformation behavior and deformation mechanism of BT25y alloy. In the present work, a series of isothermal compression tests of BT25y alloy with a height reduction of 60 % were performed in the temperature range of 1,213–1,293 K and strain rate range of 0.001–1 s^{-1} on a Gleeble-1500 thermo-mechanical simulator. Based on the stress–strain curves, the constitutive relationship and dynamic recrystallization kinetic model were established. The microstructural evolution and deformation mechanism under different deformation temperatures and strain rates were analyzed.

Experimental materials and procedures

Sample preparation

The as-received material used in the present work is BT25y alloy bar with a diameter of 270 mm. Its chemical composition is listed in Table 1. Figure 1 presents the optical microstructure of as-received BT25y alloy. As shown in the figure, the microstructure is full of equiaxed α + β, consisting of 50 % primary α phase with the average grain size of 7 um and transformed β with the secondary lamellar α thickness of 1.1 um.

Table 1: Chemical composition of BT25y titanium alloy(mass fraction, %).

C	H	O	N	Fe	Si	W	Mo	Zr	Sn	Al	Ti
0.10	0.01	0.15	0.04	0.15	0.2	1.0	4.0	4.0	2.0	6.5	Bal

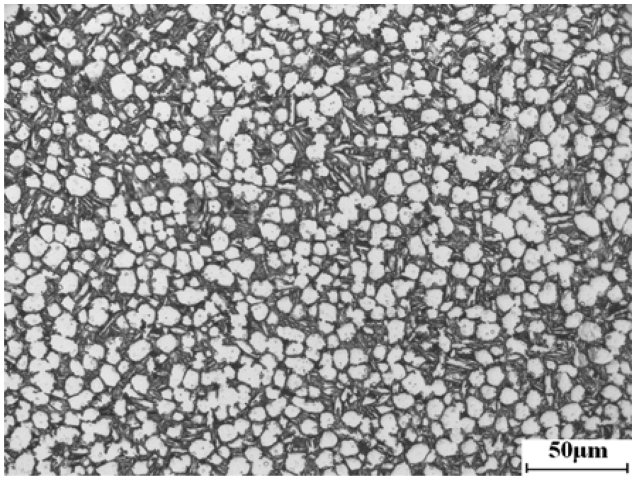

Figure 1: Microstructure of as-received BT25y titanium alloy.

Experimental procedures

The β transus temperature (T_β) of BT25y alloy was determined to be 1,253 K by metallographic phase disappearing technique. Cylindrical specimens with a diameter of 8 mm and height of 12 mm were machined. Hot compression tests were conducted on a Gleeble-1500 thermo-simulation machine at deformation temperatures of 1,213 K, 1,233 K, 1,253 K, 1,273 K, 1,293 K, and constant strain rates of 0.001 s^{-1}, 0.01 s^{-1}, 0.1 s^{-1}, 1 s^{-1}, respectively. Height reduction for the specimens was 60 %. In order to obtain a homogeneous heat distribution in the entire specimen, all the specimens were heated at a rising rate of 10 K/s and soaked for 5 min at the deformation temperature. Deformation temperature precision was controlled to ±1 K. After hot compression, the specimens were water-quenched to room temperature instantly in order to preserve the high-temperature microstructure. The load–stroke curves obtained from the compression tests were recorded and converted into true stress–strain curves automatically. The whole process of heating, holding and hot deformation was protected by argon. To examine the deformed microstructure, specimens were axially sectioned and prepared with standard method. The microstructure observation was carried out on an Olympus PM3 optical microscope (OM).

Results and discussion

High-temperature flow behavior

Figure 2 shows the true stress–strain curves of BT25y alloy at different strain rates and deformation temperatures. In the initial deformation stage, the effect of work hardening is remarkable with rapid increasing stress due to dislocation multiplication, pile-up and tangles. Each flow curve increases sharply to the peak stress at a very small strain (≤ 0.03). Once across the peak stress, the variation rules of flow curves can be divided into two cases. When deformed under low temperature and high strain rate, the flow curves present flow softening phenomenon as the flow stress drops continually with further strain after crossing the peak stress. Such flow characteristics may be attributed to deformation heating, flow instability and micro-cracking generated during hot deformation. Figure 3 shows the flow instability observed in microstructures deformed at high strain rate. At lower strain rate or higher temperature, the flow curves tend to keep steady-state after reaching the peak stress. Such steady-state curves suggest that the effect of work hardening is balanced by the flow softening mechanisms like dynamic recovery, dynamic recrystallization or superplasticity [17, 18]. Besides, the upward phenomenon can be observed at large strain of the flow curves with lower strain rate, which can be caused by the increasing friction between pressure head and tested samples during isothermal deformation.

Table 2 exhibits the effect of deformation temperature and strain rate on the peak flow stress. It could be observed that the temperature and strain rate have a significant influence on the flow stress. The peak stress decreases dramatically with increasing deformation temperature and declining strain rate, as higher temperature and lower strain rate provide longer time for energy accumulation, more stored energy for dislocation annihilation and higher boundary mobility for DRX nucleation [19, 20]. However, when deformed at lower strain rate of 0.001 s^{-1}, the effect of temperature on peak stress

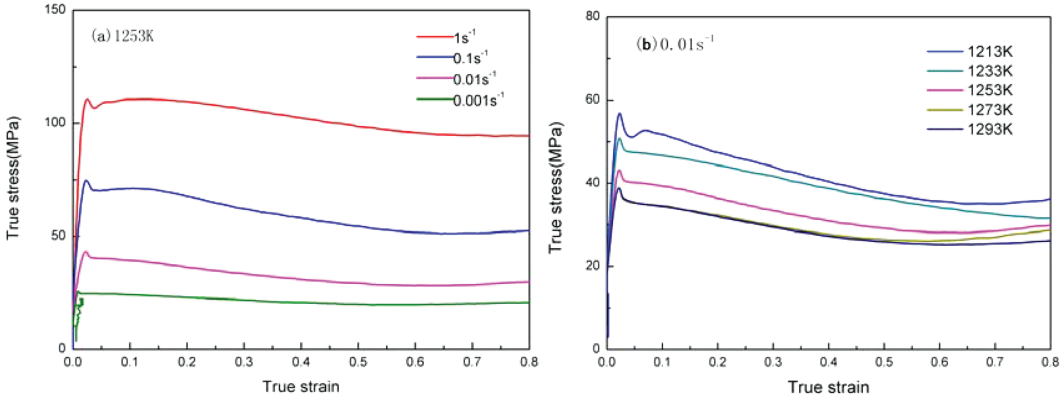

Figure 2: True stress–strain curves of BT25y alloy at different strain rates and temperatures: (a) 1,253 K; (b) 0.01 s^{-1}.

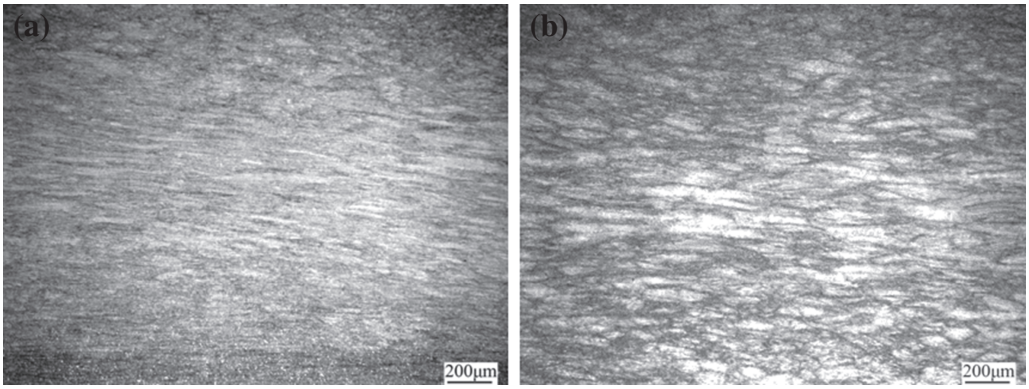

Figure 3: Microstructures with flow instability deformed at conditions of: (a) 1,233 K, 10 s^{-1}; (b) 1,253 K, 10 s^{-1}.

Table 2: Peak flow stress under different condition of hot compressive deformation (MPa).

$\dot{\varepsilon}/s^{-1}$ \ T/K	1,213	1,233	1,253	1,273	1,293
1	125.36	112.26	110.78	94.78	96.18
0.1	96.18	81.58	75.05	65.57	61.92
0.01	56.80	50.97	42.90	38.54	39.24
0.001	32.63	26.46	25.54	24.26	22.98

becomes indistinct especially at higher temperature, since it is sufficient for dynamic softening and microstructural evolution under these conditions.

Constitutive equation

Constitutive relations are often used to represent the plastic flow behavior of metals. The temperature and strain rate dependence of flow stress in hot deformation is generally expressed by the power-law using Zener-Hollomon parameter [21–23], as shown in eq. (1):

$$Z = \dot{\varepsilon}\exp(Q/RT) = A[\sinh(\alpha\sigma)]^n \tag{1}$$

Arrhenius equation is widely adopted to describe the relationships among flow stress, strain rate and temperature during high temperature plastic deformation [4]. The equation is shown as follows:

$$\dot{\varepsilon} = A[\sinh(\alpha\sigma)]^n \exp(-Q/RT) \tag{2}$$

where $\dot{\varepsilon}$ is the strain rate (s^{-1}), σ is the flow stress (MPa), R is the universal gas constant (8.314 $J.mol^{-1}.K^{-1}$), T is the absolute temperature (K), Q is the activation energy for hot deformation ($kJ.mol^{-1}$), A, α are material constants, n is stress exponent which is related to the strain rate sensitivity exponent.

In order to identify the mechanism of hot deformation, kinetic parameters like n and Q should be evaluated. Take natural logarithm of eq. (2):

$$\ln\dot{\varepsilon} = \ln A + n\ln[\sinh(\alpha\sigma)] - Q/RT \tag{3}$$

When the deformation temperature is fixed, A, Q, R and T are constants. Value of n can be obtained by calculating the partial derivative of eq. (3):

$$n = \frac{\partial \ln\dot{\varepsilon}}{\partial \ln[\sinh(\alpha\sigma)]} \tag{4}$$

When the strain rate is fixed, A, Q, R and $\dot{\varepsilon}$ are constants. Value of Q can be obtained by calculating the partial derivative of eq. (3):

$$Q = Rn\frac{\partial \ln[\sinh(\alpha\sigma)]}{\partial(1/T)} \tag{5}$$

In order to accurately describe the deformation characteristics of BT25y alloy at high temperature, peak flow stresses obtained from the true stress–strain curves are used to establish the constitutive model in this study. The value of α can be calculated by $\alpha = \beta/n_1$, where n_1 and β are taken as the average slopes of the $\ln\dot{\varepsilon}$-$\ln\sigma$ plots and $\ln\dot{\varepsilon}$-σ plots, respectively [24]. From Figure 4, values of n_1 and β are evaluated, and the value of α is determined as 0.01786 for BT25y alloy. Plots for estimating the stress exponent n are shown in Figure 5(a). The value of n is estimated to be 3.4912. Plots for estimating the deformation activation energy Q are shown in Figure 5(b). The estimated Q value is 288.0435 kJ/mol.

By taking natural logarithm on both sides of eq. (1), following formula is obtained:

$$\ln Z = \ln A + n\ln[\sinh(\alpha\sigma)] \tag{6}$$

According to the value of Q, the Z parameters under different deformation conditions can be calculated by eq. (1). The linear relationship of $\ln Z$-$\ln[\sinh(\alpha\sigma)]$ is shown in Figure 6, and the parameter $\ln A = 23.3607$ can

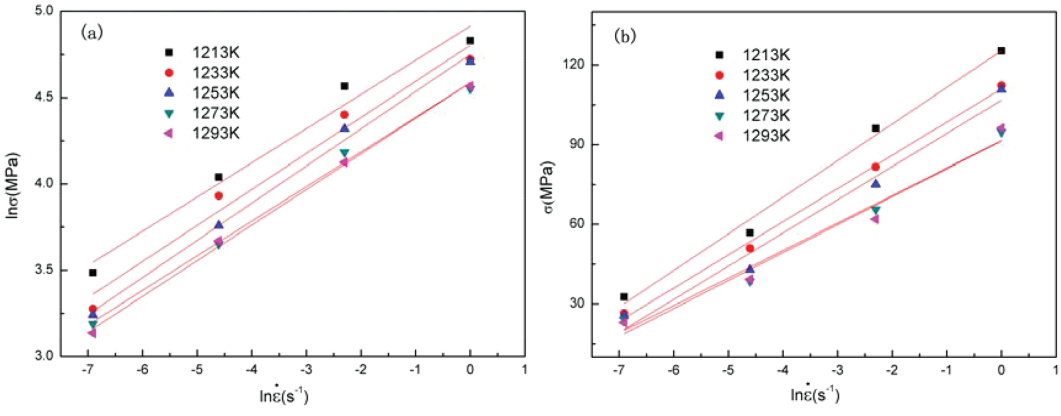

Figure 4:
(a) Relationship between $\ln\sigma$ and $\ln\dot{\varepsilon}$ at different temperatures;
(b) Relationship between σ and $\ln\dot{\varepsilon}$ at different temperatures.

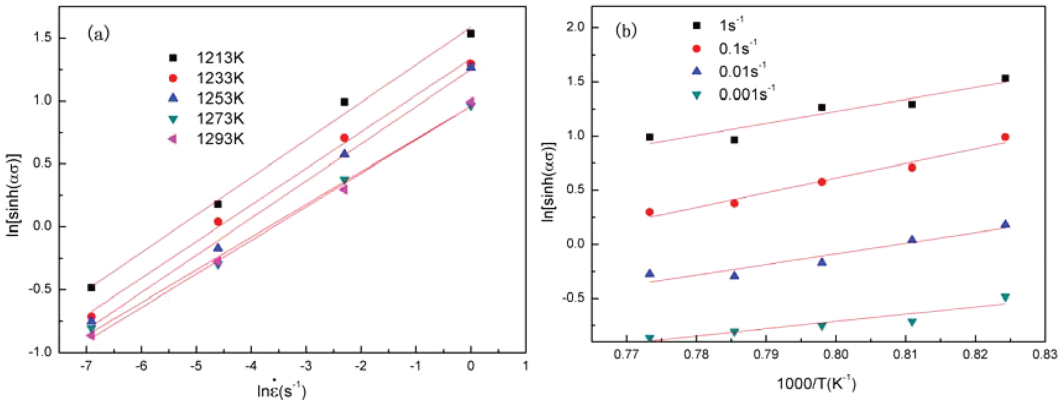

Figure 5: (a) Relationship between ln [sinh ($\alpha\sigma$)] and ln$\dot{\varepsilon}$ at different temperatures; (b) Relationship between ln [sinh ($\alpha\sigma$)] and 1,000/T at different strain rates.

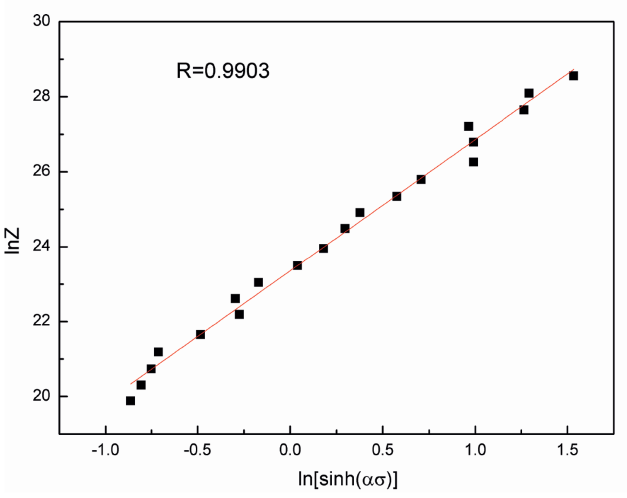

Figure 6: Relationship between ln$Z$ and ln [sinh ($\alpha\sigma$)].

be obtained by taking intercept of the fitted line. The correlation coefficient between ln$Z$ and ln[sinh($\alpha\sigma$)] reaches 0.9903, which indicates that the hyperbolic sine model between the Zener-Hollomon parameter and peak stress is suitable for describing the hot compressive deformation behavior of BT25y alloy. Thus, the calculated constitutive equation for BT25y alloy in this experiment is:

$$\dot{\varepsilon} = 1.3978 \times 10^{10} [\sinh(0.01786 \times \sigma)]^{3.49} \exp(-288.0435/RT) \quad (7)$$

By substituting $Z = \dot{\varepsilon} \exp(288.0435 \times 10^3 / 8.314T)$ into eq. (7), the flow stress can be expressed as follows:

$$\sigma = \frac{1}{0.01786} \ln\left\{ \left(\frac{Z}{1.3978 \times 10^{10}}\right)^{\frac{1}{3.49}} + \left[\left(\frac{Z}{1.3978 \times 10^{10}}\right)^{\frac{2}{3.49}} + 1\right]^{\frac{1}{2}} \right\} \quad (8)$$

While substituting deformation temperature and strain rate into eq. (8), the corresponding flow stress can be calculated. The comparison between predicted and experimental stress is shown in Figure 7. The correlation coefficient R is 0.9933, which shows the calculated values have a good agreement with experimental ones. Thus, the established constitutive equation can provide theoretical guidance for practical production in a certain sense.

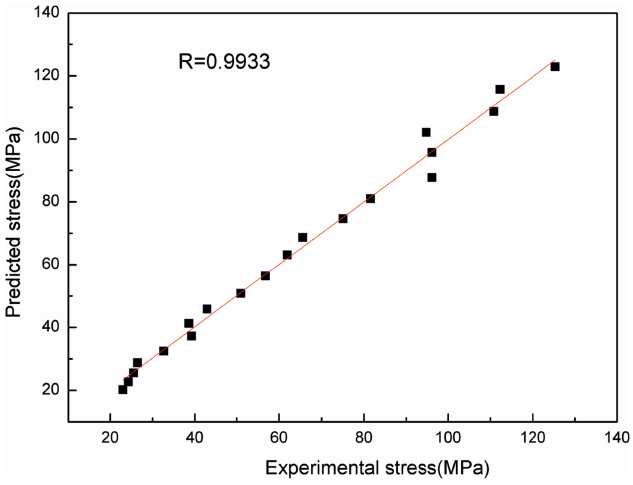

Figure 7: Comparison between predicted stress and experimental stress.

Determination of critical condition for DRX

As can be seen from Figure 2, most of the true stress–strain curves exhibit typical DRX characteristics with a peak stress at small strain followed by a gradual fall toward the steady state. However, the stress peak becomes less obvious when strain rate decreases and deformation temperature rises. Therefore, analysis of the θ–σ curves is necessarily performed to determine the

critical condition for DRX in the microstructure of BT25y alloy [25].

The values of strain hardening rate ($\theta = d\sigma/d\varepsilon$) are calculated from the true stress–strain data in Figure 2. Then the strain hardening rate values are plotted with flow stress in Figure 8 within temperatures of 1,213–1,293 K and strain rates of 0.001–1 s^{-1}. According to the approach of Poliak and Jonas [26, 27], the strain hardening rate drops to zero on the θ–σ curve while the flow curve reaches peak stress (σ_p). The inflection point of θ–σ curve corresponds to the critical stress (σ_c) for the occurrence of DRX [28, 29]. An obvious inflection is observed on almost each strain hardening rate curve in Figure 8, at which the dynamic recrystallization has already started even though the flow curve has not reached the peak stress. A typical θ–σ curve of BT25y alloy at the deformation temperature of 1,253 K and strain rate of 0.01 s^{-1} is presented in Figure 9(a). The inflection point on the θ–σ curve is accurately determined by the minimum point on the $-(d\theta/d\sigma)$ –σ curve in Figure 9(b), which is the critical stress for dynamic recrystallization. Furthermore, the critical strain can be obtained

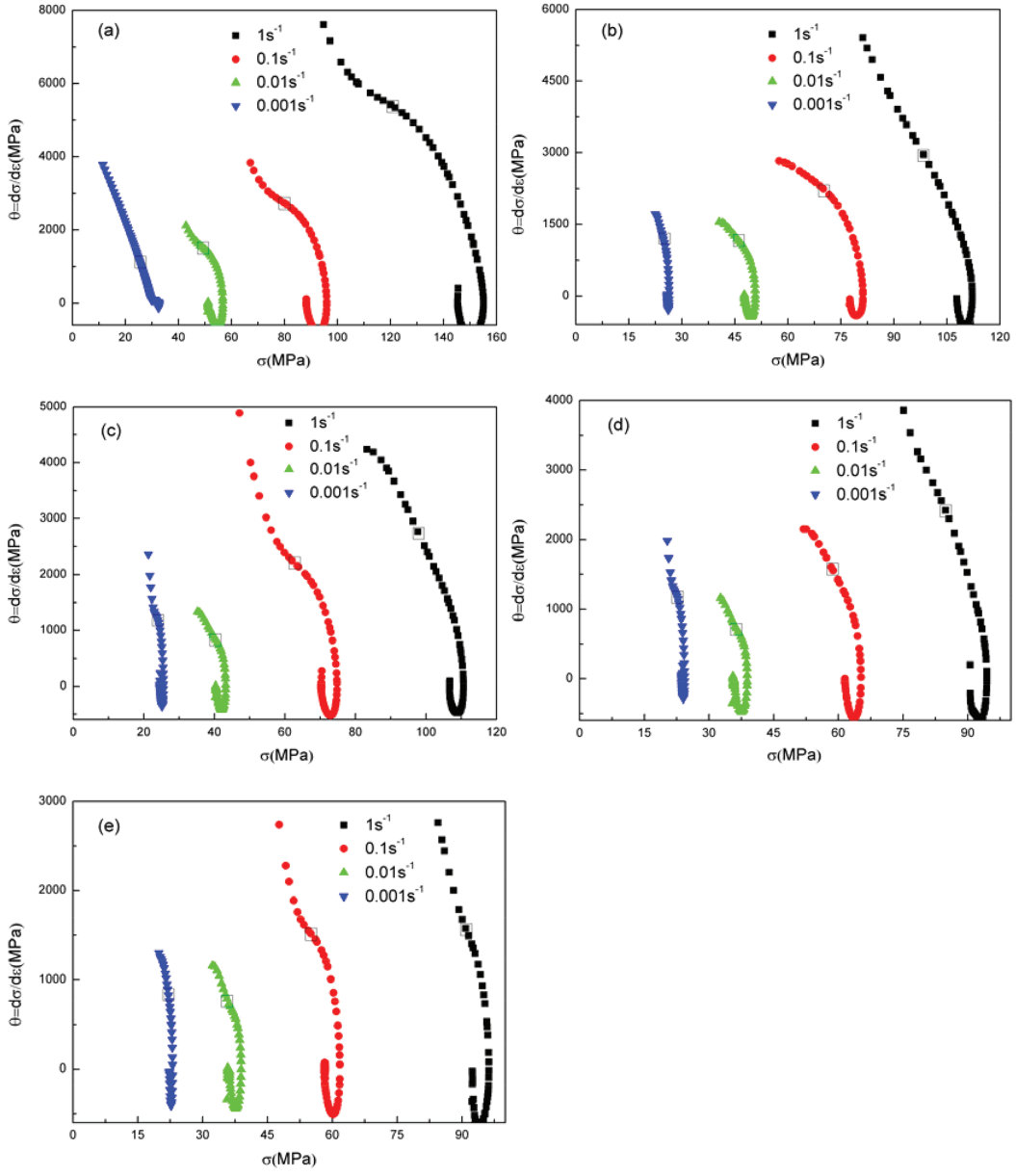

Figure 8: θ–σ curves of BT25y alloy under different deformation conditions: (a) 1,213 K; (b) 1,233 K; (c) 1,253 K; (d) 1,273 K; (e) 1,293 K.

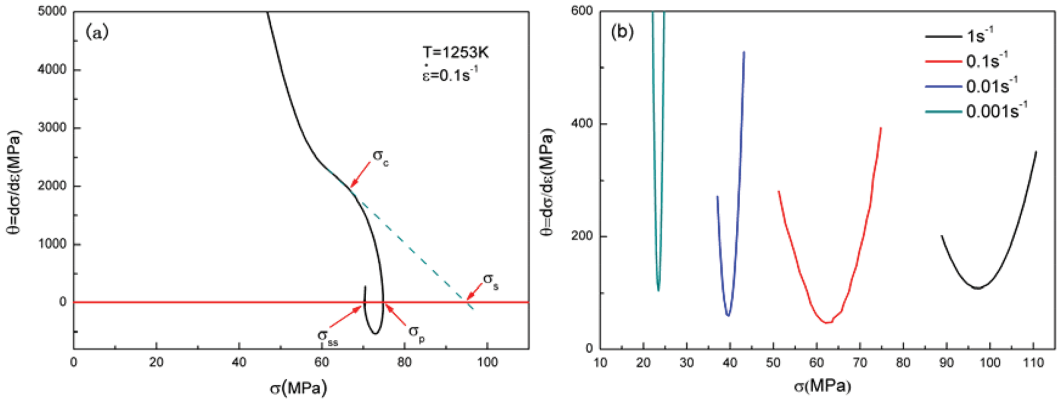

Figure 9: (a) Relationship between θ and σ at temperature of 1,253 K and strain rate of 0.01 s^{-1}; (b) Relationship between $-d\theta/d\sigma$ and σ at different strain rates under temperature of 1,253 K.

by mapping the critical stress back into the true stress-strain curves.

The measured DRX parameters are listed in Table 3. Most of the critical strain for dynamic recrystallization is less than 0.02. Moreover, the critical strain for DRX at strain rate of 0.001 s^{-1} is less than 0.01, which indicates that dynamic recrystallization occurs easily for BT25y alloy during hot compression. It can be observed from Figure 10 that the critical strain has a roughly linear relationship with the peak strain, and the fitted average value of $\varepsilon_c/\varepsilon_p$ is approximately 0.777.

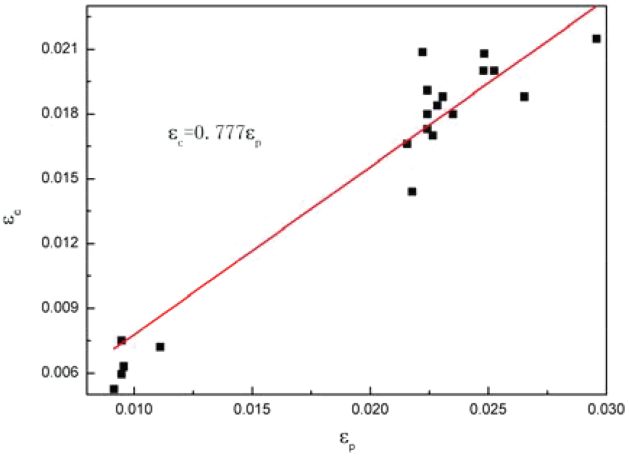

Figure 10: The relationship between ε_c and ε_p.

DRX kinetic model

The dynamic recrystallization of materials is a complex nucleation-growth process. During hot deformation, the dislocation propagates rapidly, and crystal defects like dislocation and vacancy increase significantly, which provides quantities of nucleation sites for dynamic recrystallization. When the dislocation density and accumulated distortion energy reach the critical values, the DRX occurs. In general, the initiation of DRX is judged by whether the flow curve has reached the critical strain or not. In order to establish the dynamic recrystallization kinetic model, it is

Table 3: Critical strain (ε_c) and peak strain (ε_p) for DRX at different conditions.

Strain rate/s^{-1}	Parameter	Deformation temperature/(K)				
		1,213	1,233	1,253	1,273	1,293
1.0	ε_c	0.0215	0.02	0.02	0.018	0.0191
	ε_p	0.02991	0.02789	0.02596	0.025	0.02501
0.1	ε_c	0.0208	0.0188	0.018	0.017	0.02087
	ε_p	0.02389	0.02596	0.02389	0.02389	0.02228
0.01	ε_c	0.0188	0.0184	0.0173	0.0166	0.0144
	ε_p	0.02201	0.02201	0.02201	0.02157	0.02182
0.001	ε_c	0.0072	0.0063	0.0075	0.002956	0.005254
	ε_p	0.009883	0.009584	0.009225	0.009225	0.009079

necessary to calculate the volume fraction of dynamic recrystallization (X_{DRX}) at different strains. Since the phase transition of α→β happens, the corresponding microstructure is composed of primary equiaxed α grains and transformed β phase when deformed in the two-phase field. It is very difficult to directly measure the content of dynamically recrystallized grains from the metallurgical structure. Theoretically, the X_{DRX} can be reflected from the flow stress curves. The relationship between X_{DRX} and flow stress can be expressed as follows [30–33]:

$$X_{DRX} = \frac{\sigma_{WH} - \sigma}{\sigma_s - \sigma_{ss}}, (\varepsilon \geq \varepsilon_c) \tag{9}$$

where σ_{WH} is the flow stress corresponding to different strains when DRV is the main softening mechanism, as shown in Figure 11. σ is the flow stress when DRX mechanism plays the dominant role in high-temperature plastic deformation. The saturated flow stress σ_s can be obtained by the horizontal intercept of the tangent line of θ–σ curve through the inflection point at $\theta = 0$ [34], as shown in Figure 9(a). The steady-state stress σ_{ss} can be measured from the flow stress–strain curves in Figure 2.

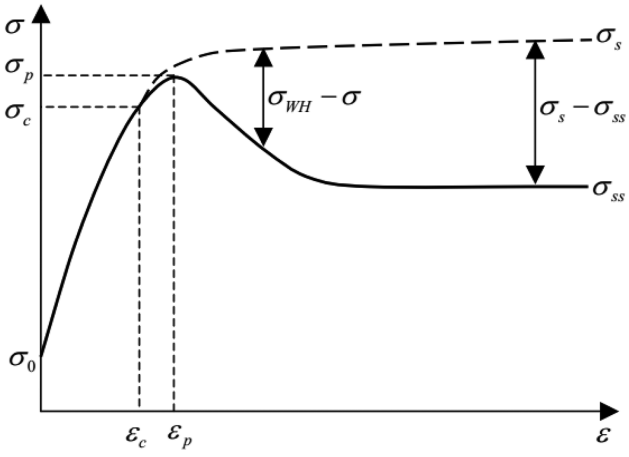

Figure 11: The calculation chart of dynamic recrystallization fraction [35].

It can be observed from Figure 2 that dynamic recrystallization is an important softening mechanism during the hot compression of BT25y alloy. The degree of DRX at a certain strain is usually described by the volume fraction of recrystallized grains in the microstructure. Based on the theory of dynamics, the correlation between X_{DRX} and ε can be expressed by the Avrami equation [36–38]:

$$X_{DRX} = 1 - \exp\left[-k_d\left(\frac{\varepsilon - \varepsilon_c}{\varepsilon_p}\right)^{n_d}\right], \quad (\varepsilon \geq \varepsilon_c) \tag{10}$$

where ε_c is the critical strain for dynamic recrystallization, ε_p is the peak strain on the true stress–strain curves, k_d is a material constant and n_d is the Avrami exponent.

After preliminary calculation by eq. (10), it can be found that the function relationship between X_{DRX} and ε at strain rate of 0.001 s^{-1} is obviously different with those of other strain rates. So the fitting calculation for different strain rates should be separated. The relationships between $\ln[-\ln(1-X_{DRX})]$ and $\ln[(\varepsilon-\varepsilon_c)/\varepsilon_p]$ are shown in Figure 12. The functional expressions are linearly fitted using the least squares method. Then the calculated results are obtained as follows:

$$X_{DRX} = 1 - \exp\left[-0.053\left(\frac{\varepsilon - \varepsilon_c}{\varepsilon_p}\right)^{1.24}\right] \quad \text{for strain rates of } 1s^{-1}, 0.1s^{-1}, 0.01s^{-1} \tag{11}$$

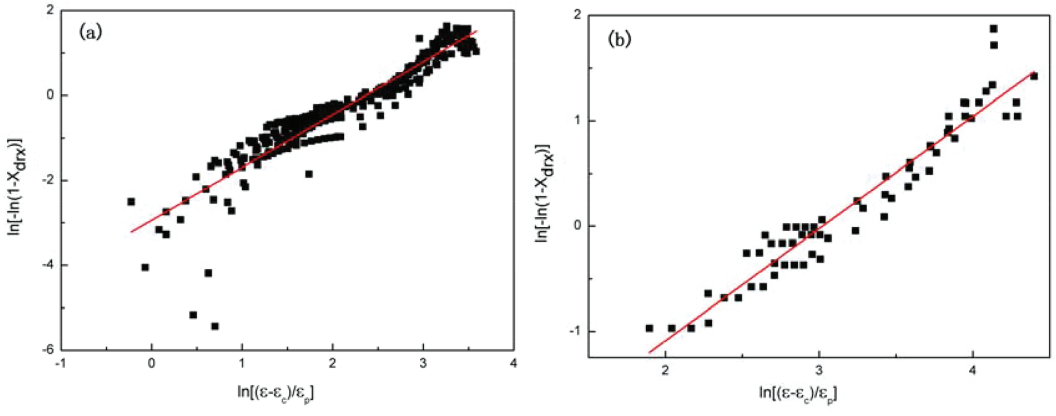

Figure 12: The relationship between $\ln[-1n(1-X_{drx})]$ and $\ln[(\varepsilon-\varepsilon_c)/\varepsilon_p]$ under strain rates of: (a) 1 s^{-1}; 0.1 s^{-1}; 0.01 s^{-1}; (b) 0.001 s^{-1}.

$$X_{DRX} = 1 - \exp\left[-0.04\left(\frac{\varepsilon - \varepsilon_c}{\varepsilon_p}\right)^{1.1}\right] \quad \text{for strain rate of } 0.001\text{s}^{-1} \tag{12}$$

Put critical strain and peak strain under different deformation conditions into corresponding DRX kinetic model, effects of deformation temperature, strain rate and strain on the X_{DRX} are shown in Figure 13. As can be seen from the figure, the volume fraction of dynamic recrystallization presents S-shaped logistic growth mode. The DRX occurs when deformation strain is less than 0.03. Even more, DRX happens before the strain reaching 0.01 when deformed at the strain rate of 0.001 s^{-1}. The DRX kinetic curves initially increase with a large slope until the X_{DRX} reaches 50 %, then the curves begin to rise with a small slope as far as the X_{DRX} reaches a constant value of 1 and the DRX process completes. The comparisons among these kinetic curves exhibit that the X_{DRX} increases with dropping strain rate for a fixed deformation temperature and strain. While for certain strain rate and strain, the X_{DRX} increases with elevated temperature. This phenomenon indicates that the dynamic recrystallization of BT25y alloy is delayed

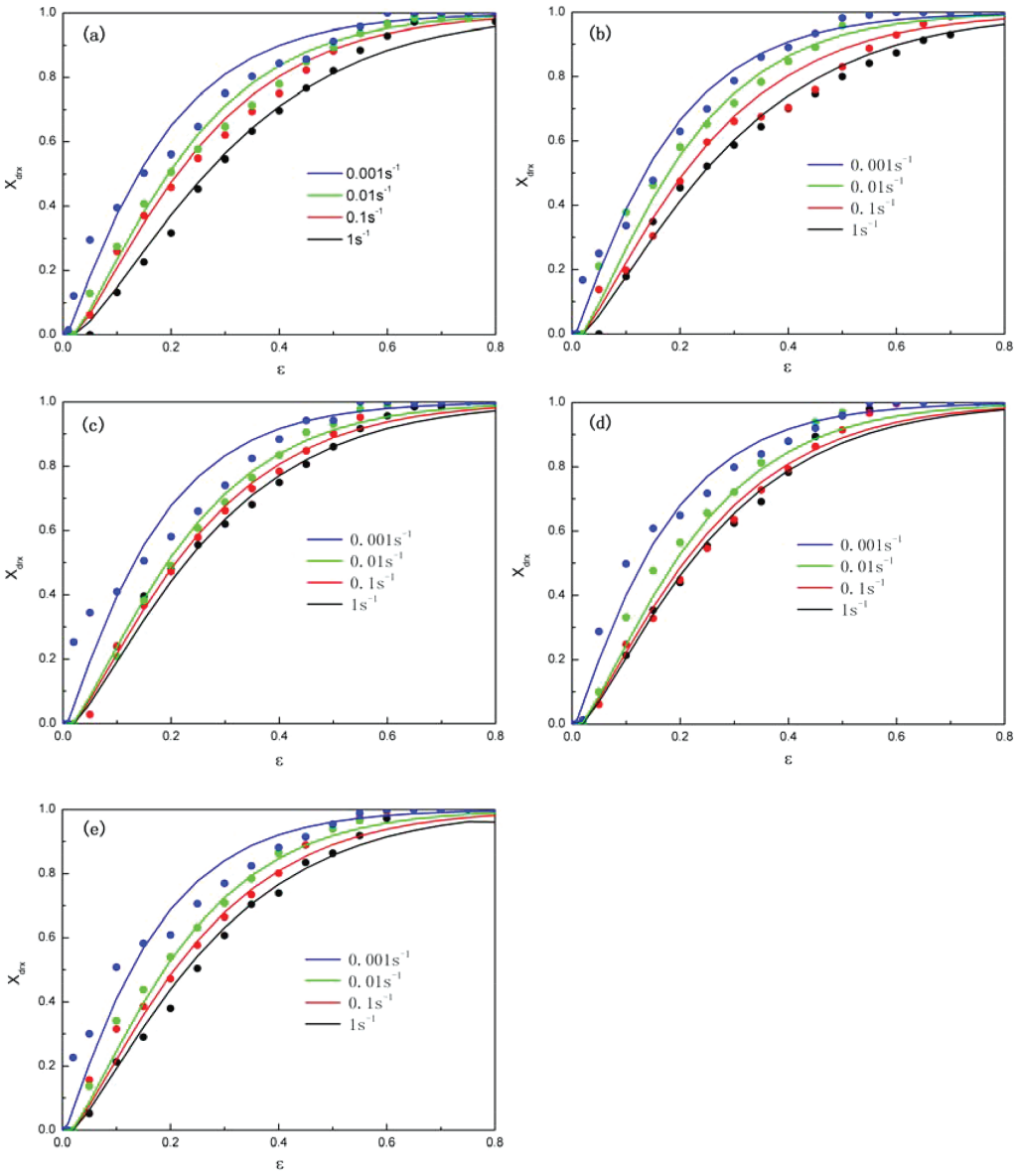

Figure 13: Comparison between measured and predicted X_{DRX} under deformation temperatures of: (a) 1,213 K; (b) 1,233 K; (c) 1,253 K; (d) 1,273 K; (e) 1,293 K. (The symbols represent measured results, the curves represent predicted results).

significantly at high strain rate and low deformation temperature. Due to the low grain boundary mobility, the dynamic recrystallization rate is much slower under low deformation temperature and high strain rate [39]. In order to validate the accuracy of the developed DRX kinetic models, Figure 13 shows the comparison between measured and predicted X_{DRX}. It can be concluded that the developed DRX kinetic models can well predict the X_{DRX} for BT25y alloy. Therefore, they can be used to describe the dynamic recrystallization behavior of BT25y alloy.

Microstructural evolution

The high-temperature plastic deformation has great effect on both macroscopic morphology and microstructural evolution. The microstructures with DRX grains under different strain rates and temperatures are observed on the optical microscope.

Figure 14 shows the effect of deformation temperature on the microstructure of BT25y alloy under the strain rate of 0.1 s^{-1}. It can be observed that as the deformation temperature increases, the content of primary equiaxed α with large grain size gradually reduces. Moreover, small recrystallized α grains can be observed at the triangle grain boundaries of transformed β while deformed in the two-phase field. In addition, the grains begin to coarsen with elevated temperature, and the equiaxial α disappears when the deformation temperature passes 1,253 K. When deformed at 1,213 K in α + β phase field, the grain boundaries of β phase are clearly visible but not integrated. Small amounts of equiaxed β can be observed in local area, which indicates the occurrence of dynamic recrystallization in β phase. Once the deformation temperature increases to 1,233 K, the β grain boundaries become integrated and fine acicular α precipitates within the β grains. The grain size of transformed β is non-uniform in the microstructure of 1,253 K. Both elongated and equiaxed β grains can be observed in the microstructure, and precipitated acicular α extends to intertwine with each other. Small recrystallized β grains appear at the grain boundaries of elongated grains. The microstructure characteristic of 1,273 K is almost the same with that of 1,253 K. Nevertheless, small recrystallized grains constitute a necklace structure along the elongated large β grains. Theoretically, as dynamic

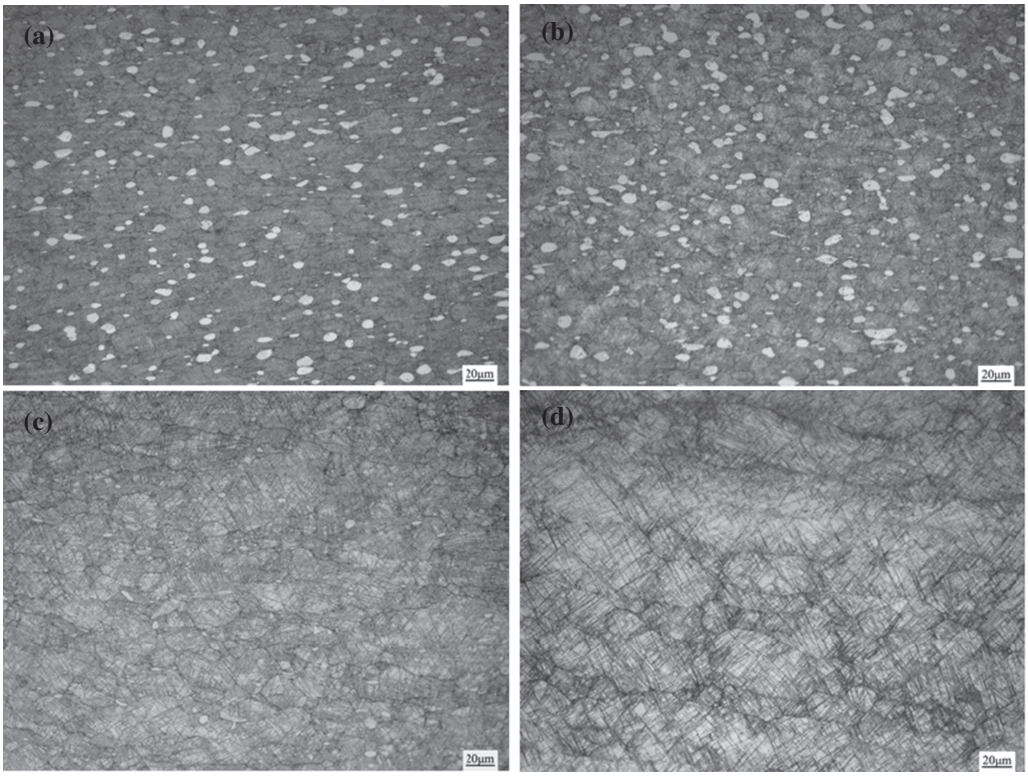

Figure 14: Microstructures under the strain rate of 0.1 s^{-1} and deformation temperatures of: (a) 1,213 K; (b) 1,233 K; (c) 1,253 K; (d) 1,273 K.

recrystallization is a thermal activation process, deformation under high temperature can provide enough stored energy and more driving force for the incidence of dynamic recrystallization. Besides, rapid diffusion of internal atom and high mobility of grain boundary under elevated temperature can accelerate the growth of DRX grains.

Figure 15 exhibits the influence of strain rate on the microstructure under the deformation temperature of 1,213 K. It can be observed that the grain growth of transformed β is apparently limited with increased strain rate. As is known to all, the flow softening process especially dynamic recrystallization is time-dependent, thus it will restrain the growth of dynamically recrystallized grains when deformed under high strain rates. While deformed at the strain rate of 1.0 s^{-1}, large amounts of primary α grains can be observed, and the grains are elongated along the direction perpendicular to the compressive deformation. Besides, small equiaxed β grains with clear grain boundaries cover the matrix, which suggests the occurrence of dynamic recrystallization in β phase. When the strain rate decreases to 0.1 s^{-1}, the primary α grains are still slightly elongated, and fine recrystallized α appears at the triangle grain boundaries of transformed β. The β grains begin to grow up, with visible but fragmented grain boundaries. Besides, thin acicular α precipitates on the matrix during the water-quenching after hot deformation. As the strain rate falls to 0.01 s^{-1}, more primary equiaxed α transforms into β phase with prolonged deformation time, and secondary lamellar α with thicker width fills the transformed β. Besides, the grain boundaries of transformed β are incomplete and unclear due to the abundance of lamellar α. Once the strain rate reaches 0.001 s^{-1}, the grains grow up further, and dynamic recrystallization occurs completely on the β matrix.

Conclusions

The thermal simulation compression tests were performed on BT25y alloy under different deformation conditions. Then the true stress–strain data were carefully analyzed. Finally, conclusions can be drawn as follows:

1 The dynamic recrystallization mechanism plays an important role in the hot working of BT25y alloy. The peak stress shows an upward tendency with dropping deformation temperature or increasing strain rate. The calculated activation energy is 288.0435 kJ/mol.

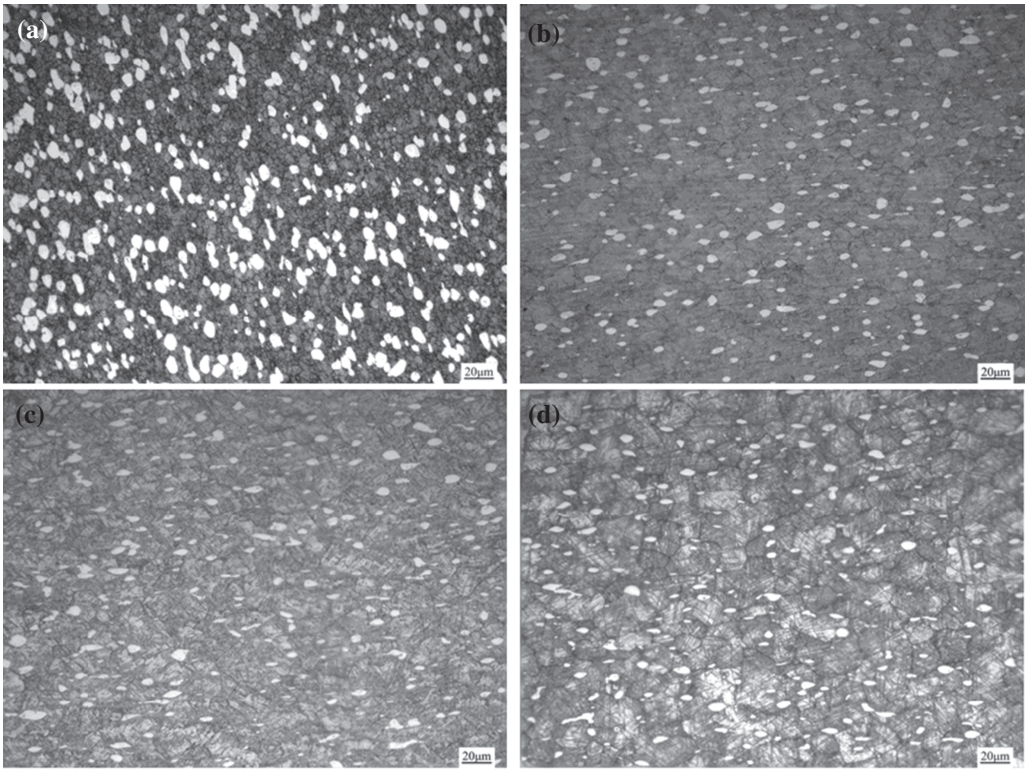

Figure 15: Microstructures under the deformation temperature of 1,213 K and strain rates of: (a) 1.0 s^{-1}; (b) 0.1 s^{-1}; (c) 0.01 s^{-1}; (d) 0.001 s^{-1}.

2 The critical stress for DRX initiation can be identified from the inflection point on the strain hardening rate curves. Then the critical strain can be measured from the flow stress curves. A linear relationship between critical strain and peak strain can be obtained, i. e., $\varepsilon_c/\varepsilon_p = 0.777$.

3 The dynamic recrystallization kinetic models are established based on the Avrami equation. The DRX volume fraction of BT25y alloy can be expressed as follows:

$$X_{DRX} = 1 - \exp\left[-0.053\left(\frac{\varepsilon - \varepsilon_c}{\varepsilon_p}\right)^{1.24}\right]$$

for strain rates of $1s^{-1}$, $0.1s^{-1}$, $0.01s^{-1}$;

$$X_{DRX} = 1 - \exp\left[-0.04\left(\frac{\varepsilon - \varepsilon_c}{\varepsilon_p}\right)^{1.1}\right]$$

for strain rate of $0.001s^{-1}$.

5 The effects of deformation temperature and strain rate on dynamic recrystallization are significant. Elevated deformation temperature or decreased strain rate can contribute to dynamic recrystallization and grain coarsening.

Funding: The work is supported by National Natural Science Foundation of China (Grant No. 51205319).

References

[1] V.N. Moiseyev, Titanium Alloys: Russian Aircraft and Aerospace Applications, CRC Press, New York (2006).
[2] K.X. Wang, W.D. Zeng, Y.Q. Zhao, Y.J. Lai and Y.G. Zhou, Mater. Sci. Eng. A, 527 (2010) 2559–2566.
[3] D. Samantaray, S. Mandal, C. Phaniraj and A.K. Bhaduri, Mater. Sci. Eng. A, 528 (2011) 8565–8572.
[4] C.M. Sellars, Mater. Sci. Technol., 6 (1990) 1072–1081.
[5] C.P. Hong and J.J. Park, J. Mater. Process. Technol., 134 (2003) 758–763.
[6] C.X. Yue, L.W. Zhang, S.L. Liao and H.J. Gao, Comput. Mater. Sci., 45 (2009) 462–466.
[7] M. Arribas, B. López and J.M. Rodriguez-Ibabe, Mater. Sci. Eng. A, 485 (2008) 383–394.
[8] Y.C. Lin and M.S. Chen, J. Mater. Process. Technol., 209 (2009) 4578–4583.
[9] A. Momeni and S.M. Abbasi, Mater. Des., 31 (2010) 3599–3604.
[10] L.X. Li, Y. Lou, L.B. Yang, D.S. Peng and K.P. Rao, Mater. Des., 23 (2002) 451–457.
[11] Y. Nan, Y.Q. Ning, H.Q. Liang, H.Z. Guo, Z.K. Yao and M.W. Fu, Mater. Des., 82 (2015) 84–90.
[12] G.Z. Quan, G.C. Luo, J.T. Liang, D.S. Wu, A. Mao and Q. Liu, Comput. Mater. Sci., 97 (2015) 136–147.
[13] K. Tan, J. Li, Z.J. Guan, J.B. Yang and J.X. Shu, Mater. Des., 84 (2015) 204–211.
[14] H.Q. Liang, H.Z. Guo, K. Tan, Y.Q. Ning, X. Luo, G. Cao, J.J. Wang and P.L. Zhen, Mater. Sci. Eng. A, 638 (2015) 357–362.
[15] C. Wu, H. Yang and H.W. Li, Trans. Nonferrous Met. Soc. China, 24 (2014) 1819–1829.
[16] X.G. Fan, H. Yang, P.F. Gao, R. Zuo and P.H. Lei, J. Mater. Process. Technol., 234 (2016) 290–299.
[17] T. Seshacharyulu, S.C. Medeiros, W.G. Frazier and Y.V.R.K. Prasad, Mater. Sci. Eng. A, 284 (2000) 184–194.
[18] W.J. Jia, W.D. Zeng, Y.G. Zhou, J.R. Liu and Q.J. Wang, Mater. Sci. Eng. A, 528 (2011) 4068–4074.
[19] Y.C. Lin and X.M. Chen, Mater. Des., 32 (2011) 1733–1759.
[20] Y.C. Lin, M.S. Chen and J. Zhang, Mater. Sci. Eng. A, 499 (2009) 88–92.
[21] T. Seshacharyulu, S.C. Medeiros, J.T. Morgan, J.C. Malas, W.G. Frazier and Y.V.R.K. Prasad, Mater. Sci. Eng. A, 279 (2000) 289–299.
[22] M. Long and H.J. Rack, Mater. Sci. Eng. A, 194 (1995) 99–111.
[23] T. Seshacharyulu, S.C. Medeiros, W.G. Frazier and Y.V.R.K. Prasad, Mater. Sci. Eng. A, 325 (2002) 112–125.
[24] X. Xiao, G.Q. Liu, B.F. Hu, X. Zheng, L.N. Wang, S.J. Chen and A. Ullah, Comput. Mater. Sci., 62 (2012) 227–234.
[25] E.I. Poliak and J.J. Jonas, ISIJ Int., 43 (2003) 684–691.
[26] E.I. Poliak and J.J. Jonas, Acta Mater., 44 (1996) 127–136.
[27] J.J. Jonas and E.I. Poliak, Mater. Sci. Forum., 426-432 (2003) 57–66.
[28] M. Shaban and B. Eghbali, Mater. Sci. Eng. A, 527 (2010) 4320–4325.
[29] H. Mirzadeh and A. Najafizadeh, Mater. Des., 31 (2010) 1174–1179.
[30] Y.W. Xu, D. Tang, Y. Song and X.G. Pan, Mater. Des., 36 (2012) 275–278.
[31] G.Z. Quan, D.S. Wu, G.C. Luo, Y.F. Xia, J. Zhou, Q. Liu and L. Gao, Mater. Sci. Eng. A., 589 (2014) 23–33.
[32] B.J. Lv, J. Peng, Y.J. Wang, X.Q. An, L.P. Zhong, A.T. Tang and F.S. Pan, Mater. Des., 53 (2014) 357–365.
[33] M. Matsuda, S. Li, Y. Kawamura, Y. Ikuhara and M. Nishida, Mater. Sci. Eng. A, 393 (2005) 269–274.
[34] X.M. Chen, Y.C. Lin, D.X. Wen, J.L. Zhang and M. He, Mater. Des., 57 (2014) 568–577.
[35] S.J. Chen, Study on Characteristics of Heavy Forging Material 30Cr2Ni4MoV Steel in Hot Deformation, Shanghai Jiaotong University, Shanghai (2009), pp. 40–44.
[36] J. Wang, H. Xiao, H.B. Xie, X.M. Xu and Y.N. Gao, Mater. Sci. Eng. A, 539 (2012) 294–300.
[37] Z.Y. Zeng, L.Q. Chen, F.X. Zhu and X.H. Liu, J. Mater. Sci. Technol., 27 (2011) 913–919.
[38] M.H. Wang, Y.F. Li, W.H. Wang, J. Zhou and A. Chiba, Mater. Des., 45 (2013) 384–392.
[39] T.C. Xu, X.D. Peng, J. Qin, Y.F. Chen, Y. Yang and G.B. Wei, J. Alloys Compd., 639 (2015) 79–88.